Computational Modeling of Planar Epileptic Waves Under Ephaptic Coupling for Closed-Loop Stimulation*

Feng Zhang[1], Meili Lu[2], Xile Wei[3]

***Abstract*— Epileptic waves in the hippocampus exhibit complex propagation patterns, which may involve nonsynaptic mechanisms, posing challenges for precise seizure localization and control. This study proposes a computational model of hippocampal pyramidal neuron network to investigate the role of ephaptic coupling in the generation and propagation of epileptic waves. Using three-compartment neuron model with orthogonal ephaptic coupling, we successfully replicate fast-slow compound epileptic waves that propagate in a planar manner. Simulations reveal that reducing the edge-to-edge distance between cells can trigger spontaneous waves, while differences in coupling strength across transverse and longitudinal directions shape wavefront propagation patterns. Furthermore, applying a closed-loop counteracting electric field can effectively slow or block the propagation of epileptic waves.**

***Clinical relevance*—These findings elucidate nonsynaptic mechanisms underlying epileptic waves and highlight ephaptic coupling as a key mechanism for seizure control, which can guide closed-loop stimulation protocol for epilepsy treatment.**

***Keywords*—Epilepsy, Ephaptic coupling, Computational modeling, Neural wave, Closed-loop stimulation**

I. INTRODUCTION

Epilepsy is a chronic neurological disorder affecting approximately 1% of the global population, with nearly 30% of cases resistant to antiepileptic drugs [1]. For these patients, surgical resection and neuromodulation are the primary treatment options. However, accurately localizing the epileptogenic zones (EZs) remains a major challenge in clinical practice [2]. Elucidating the mechanisms underlying seizure generation and propagation is therefore essential—not only to improve the precision of EZ localization and enhance surgical outcomes, but also to advance neuromodulation techniques to effectively suppress epileptiform activities.

Epileptiform activities propagating through the cerebral cortex and hippocampus can give rise to characteristic epileptic waves [3]. Recent electrophysiological studies using *in vitro* hippocampal slices have identified essential features of these waves, showing that during seizures, neural waves with distinct speeds and directions can coexist, collectively referred to as *fast-slow compound epileptic waves* [4]. In particular, slow waves are associated with dendritic calcium-mediated discharges, while fast waves are linked to N-methyl-D-aspartate (NMDA) receptor-mediated discharges [5]. Moreover, slow waves often serve as the source initiating fast waves. These findings are consistent with observations in human focal epilepsy, in which epileptiform activities originate from slowly moving EZs and rapidly spread to adjacent propagation zones [6]. Clinical studies further indicate that resecting brain regions exhibiting slow-wave characteristics improves surgical outcomes, underscoring the correlation between slow waves and EZs [7].

However, isolating EZs through cortical incisions does not always guarantee favorable surgical outcomes [8]. This discrepancy suggests that additional nonsynaptic mechanisms may contribute to seizure propagation. One compelling explanation lies in ephaptic coupling—a key nonsynaptic process whereby endogenous electric fields generated by neuronal discharges recruit neighboring neurons [9]. This mechanism is particularly prominent in high-density neuronal structures such as the hippocampus [10][11]. Experimental studies have demonstrated that both physiological and pathological discharges in the hippocampus can propagate in the absence of synaptic transmission, indicating that ephaptic coupling alone can sustain epileptiform activities [12][13]. Computational modeling further corroborates these findings, showing that fast-slow compound waves can propagate purely through ephaptic coupling [5].

Despite such progress in understanding epileptic wave propagation under ephaptic coupling, important questions remain unresolved, particularly considering the critical role of slow waves in fast-slow compound waves:

1) Under what conditions can ephaptic coupling spontaneously induce slow waves?
2) How does ephaptic coupling modulate the propagation patterns of slow waves?

To address these questions, this study extends our prior work [5] and proposes a novel hippocampal pyramidal neuron network model that integrates orthogonal ephaptic coupling. This model can reproduce fast-slow compound epileptic wave propagating in a planar manner, which closely matches experimental observations. Furthermore, we explore a closed-loop electric field stimulation strategy to suppress slow-wave propagation, offering a potential approach for seizure control. Overall, this study provides a novel perspective for investigating seizure mechanisms and advancing therapeutic approaches.

*This work was supported by the National Natural Science Foundation of China under Grant 62171312, 62271348, and the Tianjin Municipal Education Commission Scientific Research Project under Grant 2020KJ114.

[1]Feng Zhang is with School of Electrical and Information Engineering, Tianjin University, Tianjin 300072, China

[2]Meili Lu is with School of Information Technology Engineering, Tianjin University of Technology and Education, Tianjin 300222, China

[3]Xile Wei is with School of Electrical and Information Engineering, Tianjin University, Tianjin 300072, China (corresponding author to provide e-mail: xilewei@tju.edu.cn)

II. MATERIALS AND METHODS

A. Model Overview

The hippocampal pyramidal neuron network proposed in this study is illustrated in Fig. 1(a), which is a computational model derived from unfolded *in vitro* hippocampal slices. The network consists of 200×200 neurons arranged in a forest-like configuration, with their somata positioned in the same plane. The spherical soma of each neuron has a diameter of 17.8 μm, and the default edge-to-edge distance between adjacent somata is set to $d_e = 2.9$ μm. The X and Y axes correspond to the longitudinal and transverse directions of the hippocampus, respectively, while the Z-axis represents the tissue thickness along the cellular axial direction.

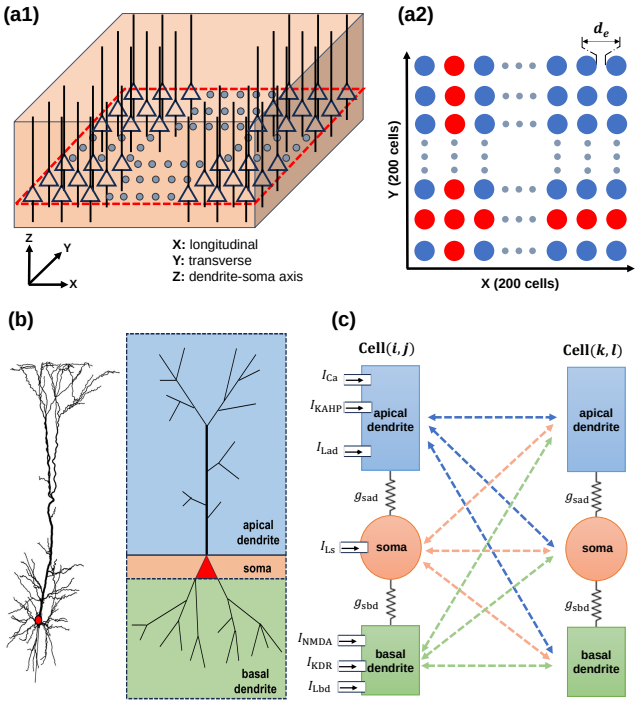

Fig. 1. **(a)** Schematic of the hippocampal pyramidal neuron network model. Panel (a1) provides a 3-D view of the model, which comprises 200×200 neurons, with their somata lying in the same (X, Y) plane. Panel (a2) shows a top-down view of this network in the (X, Y)-plane, with the locations of somata indicated by colored disks. Adjacent somata are spaced $d_e = 2.9$ μm apart (edge-to-edge). **(b)** Three-compartment pyramidal neuron model in this network, which consists of apical dendrite, soma, and basal dendrite. **(c)** Ephaptic coupling between two neurons. Cell(i, j) and Cell(k, l) represent any two neurons in the network with their coordinates satisfying $i = k$ or $j = l$.

B. Pyramidal Neuron Model: Three-Compartment Model

Each pyramidal neuron in the network is modeled as a three-compartment model, as depicted in Fig. 1(b). The model consists of the apical dendrite, soma, and basal dendrite, which capture the topological structure of realistic pyramidal neurons. The ionic currents included in each compartment are illustrated in Fig. 1(c). It should be noted that the soma compartment contains no active ion channels, as fast–slow compound epileptic waves are primarily generated by dendritic firing activities, with minimal contribution from Na^+ action potentials [5]. For model simplification, active soma currents are therefore omitted.

The membrane potentials $V_{\rm ad}$, $V_{\rm s}$, and $V_{\rm bd}$ of the apical dendrite, soma, and basal dendrite are described as follows:

$$C\frac{dV_{\rm ad}}{dt} = -I_{\rm Ca} - I_{\rm KAHP} - I_{\rm Lad} + \frac{g_{\rm sad}}{A_{\rm ad}}(V_{\rm s} - V_{\rm ad}), \tag{1}$$

$$C\frac{dV_{\rm s}}{dt} = -I_{\rm Ls} + \frac{g_{\rm sad}}{A_{\rm s}}(V_{\rm ad} - V_{\rm s}) + \frac{g_{\rm sbd}}{A_{\rm s}}(V_{\rm bd} - V_{\rm s}), \tag{2}$$

$$C\frac{dV_{\rm bd}}{dt} = -I_{\rm NMDA} - I_{\rm KDR} - I_{\rm Lbd} + \frac{g_{\rm sbd}}{A_{\rm bd}}(V_{\rm s} - V_{\rm bd}), \tag{3}$$

where $A_{\rm ad}$, $A_{\rm s}$, and $A_{\rm bd}$ are the membrane areas of the apical dendrite, soma, and basal dendrite, respectively, C is the membrane capacitance, and $g_{\rm sad}$ and $g_{\rm sbd}$ are the axial conductances. $I_{\rm Lad}$, $I_{\rm Ls}$, and $I_{\rm Lbd}$ represent passive leak currents. In the apical dendrite, $I_{\rm Ca}$ and $I_{\rm KAHP}$ are calcium current and calcium-dependent afterhyperpolarization (AHP) potassium current, respectively, which are responsible for dendritic Ca^{2+} firing. In the basal dendrite, $I_{\rm NMDA}$ and $I_{\rm KDR}$ are NMDA receptor-mediated current and delayed rectifier potassium current, respectively, responsible for dendritic NMDA firing. These active ionic currents are described using the Hodgkin-Huxley formalism as follows:

$$I_{\rm Ca} = g_{\rm Ca} \cdot m_{\rm Ca}^2 \cdot h_{\rm Ca} \cdot (V_{\rm ad} - E_{\rm Ca}), \tag{4}$$

$$I_{\rm KAHP} = g_{\rm KAHP} \cdot q \cdot (V_{\rm ad} - E_{\rm K}), \tag{5}$$

$$I_{\rm Lad} = g_{\rm Lad} \cdot (V_{\rm ad} - E_{\rm L}), \tag{6}$$

$$I_{\rm Ls} = g_{\rm Ls} \cdot (V_{\rm s} - E_{\rm L}), \tag{7}$$

$$I_{\rm NMDA} = g_{\rm NMDA} \cdot B(V_{\rm bd}) \cdot (V_{\rm bd} - E_{\rm NMDA}), \tag{8}$$

$$I_{\rm KDR} = g_{\rm KDR} \cdot n^4 \cdot (V_{\rm bd} - E_{\rm K}), \tag{9}$$

$$I_{\rm Lbd} = g_{\rm Lbd} \cdot (V_{\rm bd} - E_{\rm L}). \tag{10}$$

Here, g_x (x = Ca, KAHP, Lad, Ls, NMDA, KDR, Lbd) and E_y (y = Ca, K, L, NMDA) are the maximum conductances and reversal potentials of these ion channels, respectively. $m_{\rm Ca}$, $h_{\rm Ca}$, q, and n are dimensionless quantities related to the activation or inactivation of the ion channels, governed by:

$$\frac{dm_{\rm Ca}}{dt} = \frac{m_{\rm Ca,\infty}(V_{\rm ad}) - m_{\rm Ca}}{\tau_{m_{\rm Ca}}}, \tag{11}$$

$$\frac{dh_{\rm Ca}}{dt} = \frac{h_{\rm Ca,\infty}(V_{\rm ad}) - h_{\rm Ca}}{\tau_{h_{\rm Ca}}}, \tag{12}$$

$$\frac{dq}{dt} = \frac{q_\infty([{\rm Ca}^{2+}]_i) - q}{\tau_q}, \tag{13}$$

$$\frac{dn}{dt} = \alpha_n(V_{\rm bd}) - n\big(\alpha_n(V_{\rm bd}) + \beta_n(V_{\rm bd})\big), \tag{14}$$

In (13), $[{\rm Ca}^{2+}]_i$ is dimensionless and proportional to the Ca^{2+} concentration adjacent to the membrane, governed by:

$$\frac{d[{\rm Ca}^{2+}]_i}{dt} = -0.13 I_{\rm Ca} - \frac{[{\rm Ca}^{2+}]_i}{\tau_{[{\rm Ca}]}}. \tag{15}$$

Unless otherwise specified, all parameters are taken from Table I. Additional gating and rate functions, including $B(V_{\rm bd})$, $m_{\rm Ca,\infty}(V_{\rm ad})$, $h_{\rm Ca,\infty}(V_{\rm ad})$, $q_\infty([{\rm Ca}^{2+}]_i)$, $\alpha_n(V_{\rm bd})$, and $\beta_n(V_{\rm bd})$, are provided in Appendix.

TABLE I

PARAMETER VALUES FOR THE THREE-COMPARTMENT MODEL

Parameters	Values	Parameters	Values
E_{Ca}	10 mV	g_{Ca}	34.5 mS/cm^2
E_{K}	-80 mV	g_{KAHP}	0.03 mS/cm^2
E_{NMDA}	0 mV	g_{NMDA}	6.72 mS/cm^2
E_{L}	-70 mV	g_{KDR}	200 mS/cm^2
$\tau_{m_{\mathrm{Ca}}}$	35 ms	g_{Lad}	1.47 mS/cm^2
$\tau_{h_{\mathrm{Ca}}}$	157 ms	g_{Ls}	1.47 mS/cm^2
$\tau_{[\mathrm{Ca}]}$	13 ms	g_{Lbd}	1.28 mS/cm^2
τ_q	300 ms	g_{sad}	8.01×10^{-6} mS/cm^2
A_{ad}	9.46×10^{-5} cm^2	g_{sbd}	1.60×10^{-5} mS/cm^2
A_{s}	9.95×10^{-6} cm^2	C	1 μF/cm^2
A_{bd}	1.49×10^{-4} cm^2		

C. Orthogonal Ephaptic Coupling

To investigate the conditions for spontaneous generation and propagation patterns of epileptic waves in the context of ephaptic coupling, neuronal communication in the network is assumed to occur exclusively via endogenous electric fields. The ephaptic coupling between a source Cell(i,j) and a target Cell(k,l) is illustrated in Fig. 1(c). In extracellular tissue fluid with resistivity ρ, the extracellular potential at compartment z ($z=\mathrm{ad,s,bd}$) of the target Cell(k,l) can be computed using the quasi-static formulation of Maxwell's equations as follows [14]:

$$V_{z\_\mathrm{ex}}(k,l) = SF\cdot\frac{\rho}{4\pi}\sum_{(i,j)}\left(\frac{I_{\mathrm{tran\_ad}}(i,j)}{r_{(i,j)\_\mathrm{ad}\to(k,l)\_z}}+\frac{I_{\mathrm{tran\_s}}(i,j)}{r_{(i,j)\_\mathrm{s}\to(k,l)\_z}}+\frac{I_{\mathrm{tran\_bd}}(i,j)}{r_{(i,j)\_\mathrm{bd}\to(k,l)\_z}}\right)\quad(z=\mathrm{ad,s,bd}),\tag{16}$$

where transmembrane currents $I_{\mathrm{tran\_ad}}(i,j)$, $I_{\mathrm{tran\_s}}(i,j)$, and $I_{\mathrm{tran\_bd}}(i,j)$ from the source Cell(i,j) are separated from the target compartment z by distances $r_{(i,j)\_\mathrm{ad}\to(k,l)\_z}$, $r_{(i,j)\_\mathrm{s}\to(k,l)\_z}$, and $r_{(i,j)\_\mathrm{bd}\to(k,l)\_z}$, respectively. To calculate these distances between compartments from different neurons, the intracellular distances between the soma and its apical and basal dendrites within a neuron are set to $L_{\mathrm{sad}}=500\ \mu$m and $L_{\mathrm{sbd}}=250\ \mu$m, respectively. The extracellular resistivity ρ is set to 300 $\Omega\cdot$cm, and the "stacking factor" SF is set to 5 [15].

Because ephaptic coupling induces unequal extracellular potentials across the three compartments ($V_{\mathrm{ad\_ex}}$, $V_{\mathrm{s\_ex}}$, and $V_{\mathrm{bd\_ex}}$), (1)–(3) should be modified following [16] as:

$$C\frac{dV_{\mathrm{ad}}}{dt} = -I_{\mathrm{Ca}}-I_{\mathrm{KAHP}}-I_{\mathrm{Lad}}+\frac{g_{\mathrm{sad}}}{A_{\mathrm{ad}}}(V_{\mathrm{s\_in}}-V_{\mathrm{ad\_in}}),\tag{17}$$

$$C\frac{dV_{\mathrm{s}}}{dt} = -I_{\mathrm{Ls}}+\frac{g_{\mathrm{sad}}}{A_{\mathrm{s}}}(V_{\mathrm{ad\_in}}-V_{\mathrm{s\_in}})+\frac{g_{\mathrm{sbd}}}{A_{\mathrm{s}}}(V_{\mathrm{bd\_in}}-V_{\mathrm{s\_in}}),\tag{18}$$

$$C\frac{dV_{\mathrm{bd}}}{dt} = -I_{\mathrm{NMDA}}-I_{\mathrm{KDR}}-I_{\mathrm{Lbd}}+\frac{g_{\mathrm{sbd}}}{A_{\mathrm{bd}}}(V_{\mathrm{s\_in}}-V_{\mathrm{bd\_in}}),\tag{19}$$

where $V_{\mathrm{ad\_in}}$, $V_{\mathrm{s\_in}}$, and $V_{\mathrm{bd\_in}}$ denote the intracellular potentials of the three compartments. Using the definition of transmembrane potential, $V=V_{\mathrm{in}}-V_{\mathrm{ex}}$, (17)–(19) can be rewritten as:

$$C\frac{dV_{\mathrm{ad}}}{dt} = -I_{\mathrm{Ca}}-I_{\mathrm{KAHP}}-I_{\mathrm{Lad}}+\frac{g_{\mathrm{sad}}}{A_{\mathrm{ad}}}(V_{\mathrm{s}}-V_{\mathrm{ad}}+V_{\mathrm{s\_ex}}-V_{\mathrm{ad\_ex}}),\tag{20}$$

$$C\frac{dV_{\mathrm{s}}}{dt} = -I_{\mathrm{Ls}}+\frac{g_{\mathrm{sad}}}{A_{\mathrm{s}}}(V_{\mathrm{ad}}-V_{\mathrm{s}}+V_{\mathrm{ad\_ex}}-V_{\mathrm{s\_ex}})+\frac{g_{\mathrm{sbd}}}{A_{\mathrm{s}}}(V_{\mathrm{bd}}-V_{\mathrm{s}}+V_{\mathrm{bd\_ex}}-V_{\mathrm{s\_ex}}),\tag{21}$$

$$C\frac{dV_{\mathrm{bd}}}{dt} = -I_{\mathrm{NMDA}}-I_{\mathrm{KDR}}-I_{\mathrm{Lbd}}+\frac{g_{\mathrm{sbd}}}{A_{\mathrm{bd}}}(V_{\mathrm{s}}-V_{\mathrm{bd}}+V_{\mathrm{s\_ex}}-V_{\mathrm{bd\_ex}}).\tag{22}$$

To improve computational efficiency in simulating planar propagation of epileptic waves, ephaptic coupling is assumed to occur only along the longitudinal (X) and transverse (Y) directions. For example, as illustrated in Fig. 1(a2), Cell$(2,2)$ is ephaptically coupled only to neurons in the same row and column (indicated by red disks). That is, each neuron in the network is ephaptically coupled exclusively to the other 398 neurons in its row and column. This orthogonal ephaptic coupling scheme enables efficient simulation of planar epileptic wave propagation with reduced computational cost.

D. Simulation methods

The network model is implemented in MATLAB R2022a and numerically integrated using fourth-order Runge–Kutta algorithm with a fixed time step of 0.05 ms. All neurons are initialized with membrane potentials near the resting potential of -60 mV.

III. RESULTS

A. Reduction in Intercellular Distance Facilitates Spontaneous Fast-Slow Compound Epileptic Waves

Previous *in vitro* experiments have shown that reducing extracellular space volume by lowering extracellular osmolarity accelerates neural wave propagation [12]. Equation (16) implies that a smaller intercellular distance induces stronger extracellular potentials, which may lead to significant endogenous electric fields. Based on this, we hypothesize that reducing the intercellular distance would trigger spontaneous epileptic waves. To test this hypothesis, we locally reduce the edge-to-edge distance in the simulated network, as indicated by the *red region* in Fig. 2(a), and observed whether any discharge activity would spontaneously emerge in this region. To exclude other confounding factors, before the simulation began we confirmed that there was no spontaneous firing activity in the network with the default edge-to-edge distance (Fig. 1(a2)).

The simulated potentials of apical and basal dendrites are shown in Fig. 2(b). Approximately 900 ms after the simulation start, both apical and basal dendrites undergo spontaneous depolarization around the red region, with the apical dendrite depolarizing first. These depolarized regions then serve as sources of slow and fast waves, giving rise to spontaneous fast-slow compound waves, consistent with experimental observations in [5]. Isochrone maps of peak membrane potentials in Fig. 2(c) illustrate the planar propagation

of slow and fast waves, highlighting the positions of wave sources and the wavefront propagation patterns. Through multiple simulations, we found that the smaller the edge-to-edge distance in the red region, the faster the spontaneous formation of fast-slow compound waves (Fig. 2(d)). This trend is in agreement with experimental findings, where low osmolarity-induced cell swelling increases the excitability of hippocampal CA1 pyramidal neurons, thereby promoting epileptiform activities both *in vitro* and *in vivo* [17].

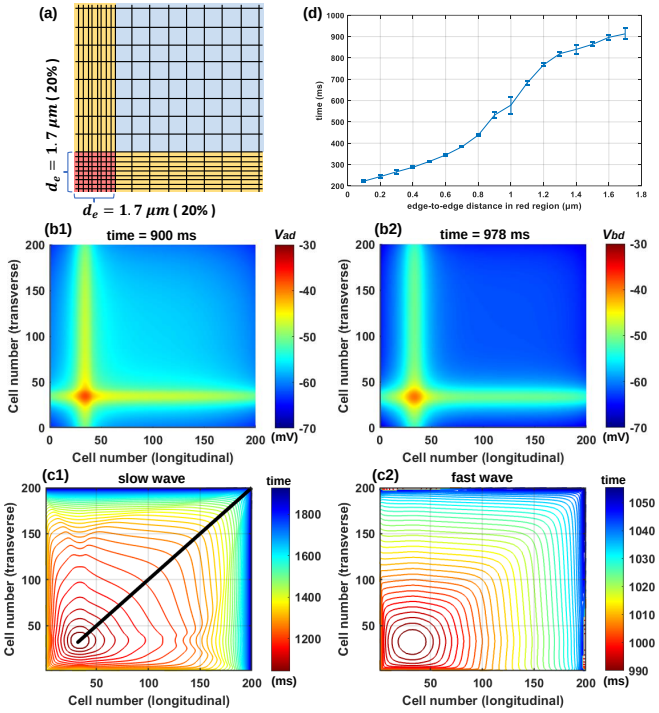

Fig. 2. **(a)** Reducing the edge-to-edge distance (d_e) in a local cell array (*red region*). In both transverse and longitudinal directions, the edge-to-edge distance of the first 20% of neurons is reduced to 1.7 μm, while the remaining 80% retain the default distance. Therefore, the red region represents the area with significant ephaptic coupling in the array. **(b)** Heatmaps of membrane potentials: (b1) apical dendrite potentials V_{ad} of all neurons at $t = 900$ ms, and (b2) basal dendrite potentials V_{bd} at $t = 978$ ms. **(c)** Isochrone maps of peak membrane potential V_{ad} (c1) and V_{bd} (c2) showing the propagation of the slow and fast wavefronts in the network. The *black line* traces the fastest propagation path of the slow wavefront. The method for generating isochrone maps follows the approach described in [4]. **(d)** Time required for the spontaneous formation of fast-slow compound waves as a function of the edge-to-edge distance in the red region.

B. Differences in Coupling Strength Across Transverse and Longitudinal Directions Shape Wavefront Propagation

Considering the correlation between slow waves and EZs, understanding the propagation patterns of slow waves is essential for predicting the potential movement of EZs. Therefore, we further investigated how ephaptic coupling influences the wavefront propagation patterns of slow waves. As shown in Fig. 2(c), the fastest propagation path of the slow wavefront is almost a straight line from the lower-left to the upper-right corner. This can be attributed to the equal edge-to-edge distance in the red region along both the X- and Y-axes (Fig. 2(a)). We then examined the effect of introducing different edge-to-edge distances along these two directions. As shown in Fig. 3(a1), the edge-to-edge distance along the Y-axis in the red region is further reduced to 1.4 μm, which strengthens ephaptic coupling in this direction. The corresponding simulation result shows that the fastest slow wavefront initially propagates along the Y-axis, then shifts toward the X-axis, and ultimately reaches the upper-right corner of the network (Fig. 3(a2)). Moreover, the shorter this edge-to-edge distance, the farther the initial propagation along the Y-axis extends (Fig. 3(a3)).

We also explored another method of strengthening ephaptic coupling by increasing the proportion of the red region. As shown in Fig. 3(b1), the proportion of the red region along the Y-axis is increased to 28%. The resulting slow wavefront propagation, shown in Fig. 3(b2), qualitatively resembles the pattern observed in Fig. 3(a2). Similarly, the larger this proportion, the farther the initial propagation along the Y-axis extends (Fig. 3(b3)). These results indicate that differences in coupling strength across transverse and longitudinal directions have a significant impact on wavefront propagation patterns. Spontaneous epileptic waves preferentially emerge along the direction with stronger ephaptic coupling, and increasing this coupling strength delays the shift in propagation direction.

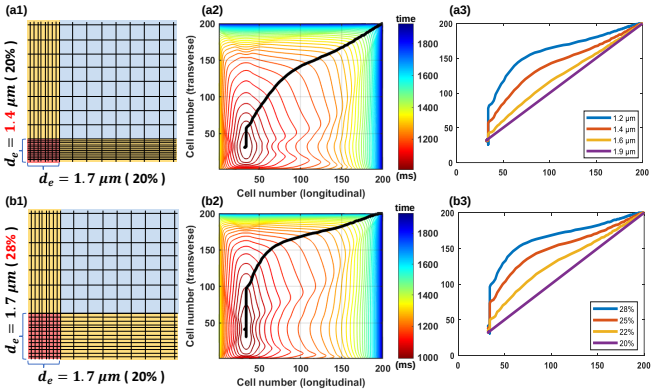

Fig. 3. **(a)** Effect of edge-to-edge distance on slow wavefront propagation. Compared to the cell array in Fig. 2(a), in panel (a1), the edge-to-edge distance along the Y-axis in the red region is reduced from 1.7 μm to 1.4 μm. Panel (a2) presents the corresponding slow wavefront propagation in the network, with the black line indicating the fastest propagation path. Panel (a3) compares the fastest propagation paths for different Y-axis edge-to-edge distance in the red region (The axis labels in panel (a3) are consistent with those in panel (a2)). **(b)** Effect of the proportion of cells in the red region on slow wavefront propagation. Compared to the cell array in Fig. 2(a), in panel (b1), the proportion of the red region along the Y-axis is increased from 20% to 28%. Panel (b2) shows the resulting slow wavefront propagation, and panel (b3) compares the fastest propagation paths for different proportions of cells in the red region along the Y-axis.

C. Closed-loop Stimulation for Blocking Wave Propagation

We have demonstrated that the strength of ephaptic coupling influences both the spontaneous formation and the propagation patterns of slow waves. At the microscopic scale, these effects arise from endogenous electric fields generated by neuronal discharges. Therefore, applying a counteracting electric field may slow or even block wave propagation. To

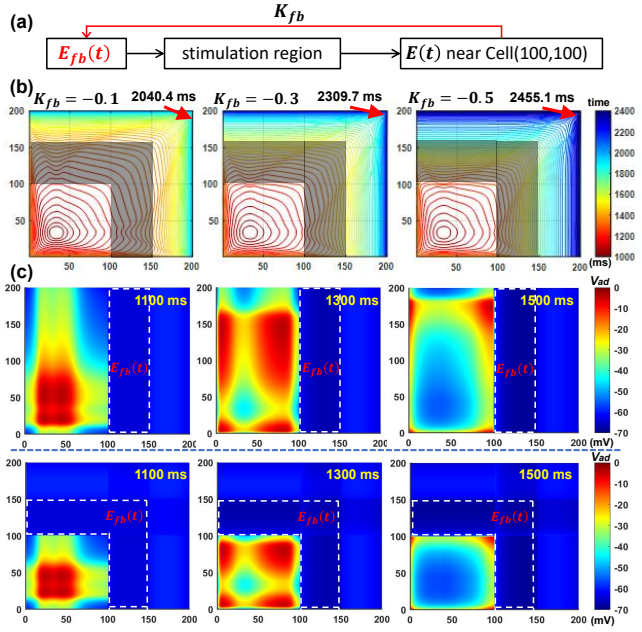

Fig. 4. **(a)** Closed-loop electric field stimulation protocol for controlling slow waves ($K_{fb} < 0$). **(b)** Simulation results with $K_{fb} = -0.1$, -0.3, and -0.5. The cell array configuration matches that in Fig. 2(a). The *shaded area* indicates the stimulation region where the negative feedback field is applied. *Red arrows* mark the time when the slow wave reaches the network boundary. **(c)** Simulation results with $K_{fb} = -0.9$, where the counteracting electric field completely blocks slow wave propagation. White dashed lines outline the stimulation region. In the first row, this region blocks propagation along the X-axis; in the second row, it blocks propagation across the X- and Y-axes.

test this hypothesis, we detect the endogenous electric field $E(t) = V_{\text{s\_ex}}(t) - V_{\text{ad\_ex}}(t)$ from an incoming slow wave and apply a proportional counteracting field, $E_{fb}(t) = K_{fb} \times E(t)$ with a negative feedback gain K_{fb} (Fig. 4(a)). Specifically, $E(t)$ is measured at the network center (Cell$(100,100)$), and the negative feedback field $E_{fb}(t)$ is applied to a stimulation region in its vicinity (shaded area in Fig. 4(b)). Since our focus is on slow-wave propagation, $E_{fb}(t)$ is applied between the apical dendrite and soma, which are responsible for slow-wave generation. In this case, for pyramidal neurons in the stimulation region, (20)–(21) are modified as follows:

$$C\frac{dV_{\text{ad}}}{dt} = -I_{\text{Ca}} - I_{\text{KAHP}} - I_{\text{Lad}} + \frac{g_{\text{sad}}}{A_{\text{ad}}}(V_{\text{s}} - V_{\text{ad}} + V_{\text{s\_ex}} - V_{\text{ad\_ex}} + E_{fb} \cdot L_{\text{sad}}), \quad (23)$$

$$C\frac{dV_{\text{s}}}{dt} = -I_{\text{Ls}} + \frac{g_{\text{sad}}}{A_{\text{s}}}(V_{\text{ad}} - V_{\text{s}} + V_{\text{ad\_ex}} - V_{\text{s\_ex}} - E_{fb} \cdot L_{\text{sad}}) + \frac{g_{\text{sbd}}}{A_{\text{s}}}(V_{\text{bd}} - V_{\text{s}} + V_{\text{bd\_ex}} - V_{\text{s\_ex}}). \quad (24)$$

Simulation results with different values of K_{fb} are shown in Fig. 4(b). It can be seen that as $|K_{fb}|$ increases, the time required for the wave to reach the network boundary also increases (marked by red arrows). In particular, at $K_{fb} = -0.9$, the counteracting field blocks propagation (Fig. 4(c)). When the stimulation region surrounds the wave source, it isolates the source from other propagation zones, maximally suppressing the spread of slow wave. These results indicate that endogenous electric fields directly modulate epileptic wave propagation speed, and suggest that closed-loop electric field clamping could effectively suppress epileptic wave propagation in the hippocampus.

IV. DISCUSSION AND CONCLUSIONS

Traditionally, studies on the mechanisms of epileptic seizures have focused primarily on synaptic coupling, with comparatively little attention given to ephaptic coupling. In recent years, however, accumulating experimental evidence has demonstrated that ephaptic coupling can independently mediate the propagation of epileptiform activity [9][12][18]. On the other hand, fast–slow compound waves, as a distinct type of epileptic wave, exhibit propagation patterns similar to those observed in human focal epilepsy. Because the slow-wave component is often correlated with the EZ, these waves have important clinical value for EZ localization. Motivated by this background, this study developed a hippocampal pyramidal neuron network model to investigate the role of ephaptic coupling in fast–slow compound waves. Compared with the prior model in [5], the proposed model expands the network size and incorporates orthogonal ephaptic coupling, enabling the simulation of planar epileptic waves and allowing direct observation of wavefront propagation patterns.

This study primarily addresses the question: under what conditions can ephaptic coupling spontaneously induce fast–slow compound waves? Simulations in Fig. 2 show that locally reducing the intercellular distance enables apical dendrites to spontaneously generate Ca^{2+} firing and basal dendrites to spontaneously generate NMDA firing, forming the fast and slow waves, respectively. The underlying mechanism can be explained as follows: in the default network configuration with normal intercellular distance (Fig. 1(a2)), no spontaneous discharges occur, but the transmembrane currents of neurons remain nonzero, generating weak endogenous electric fields. When the intercellular distance is reduced, (16) indicates that these weak fields are significantly amplified, ultimately depolarizing both apical and basal dendrites, with the apical dendrites depolarizing first. If we block apical Ca^{2+} channels (i.e., set $g_{\text{Ca}} = 0$) while keeping basal NMDA channels open, both waves disappears (data not shown). Therefore, in spontaneous fast–slow compound waves, the slow wave acts as the source that triggers the fast wave. This causal relationship is consistent with experimental observations [4][5], and thus the slow wave was chosen as the primary focus of this study.

From the perspective of epilepsy pre-surgical evaluation, these findings may provide novel insights into the clinical EZ localization. For example, in hippocampal regions where extracellular osmolarity is abnormally reduced, neuronal swelling may decrease intercellular spacing, making these regions potential EZs [17]. Furthermore, simulations in Fig. 3 demonstrate that differences in coupling strength between the transverse and longitudinal directions can markedly influence slow-wave propagation patterns. Particularly, spontaneous waves preferentially emerge along the direction with stronger coupling. This suggests that when predicting the migration

pathways of EZs within the hippocampus, anisotropy of the pyramidal network should be taken into account. EZs may migrate slowly along regions with higher neuronal density or lower osmolarity. To counteract this, we proposed a closed-loop electric field stimulation strategy to suppress the propagation of slow waves. As shown in Fig. 4, applying a counteracting electric field around the slow-wave source can weaken ephaptic coupling and thereby slow or block the spread of the slow wave, effectively suppressing fast–slow compound waves.

In conclusion, this study elucidates nonsynaptic mechanisms underlying fast–slow compound epileptic waves and identifies ephaptic coupling as a key target for seizure control. The results provide a theoretical basis for designing closed-loop stimulation protocols for epilepsy treatment. In future work, we plan to incorporate additional coupling mechanisms, such as chemical synapses, gap junctions [19], and K^+ diffusion coupling [20], to examine the role of ephaptic coupling in epileptic wave dynamics under more physiologically realistic conditions. This could increase the potential clinical applicability of our findings.

APPENDIX

Here, we present the gating and rate functions in the three-compartment model. In the apical dendrite, m_{Ca} and h_{Ca} represent the activation and inactivation gating variables of I_{Ca}, respectively. Their steady-state functions, $m_{\mathrm{Ca},\infty}(V_{\mathrm{ad}})$ and $h_{\mathrm{Ca},\infty}(V_{\mathrm{ad}})$, are given in Boltzmann form as follows:

$$\begin{aligned} m_{\mathrm{Ca},\infty}(V_{\mathrm{ad}}) &= 1/(1+\exp(-(V_{\mathrm{ad}}+20)/16)), \\ h_{\mathrm{Ca},\infty}(V_{\mathrm{ad}}) &= 1/(1+\exp((V_{\mathrm{ad}}+40)/7)). \end{aligned}$$

For the activation gating variables q of I_{KAHP}, its steady-state function $q_\infty([\mathrm{Ca}^{2+}]_i)$ is as follows [21]:

$$q_\infty([\mathrm{Ca}^{2+}]_i) = \frac{1}{1+81/[\mathrm{Ca}^{2+}]_i^4},$$

In the basal dendrite, the activation gating variable n for I_{KDR} has rate founctions $\alpha_n(V_{\mathrm{bd}})$ and $\beta_n(V_{\mathrm{bd}})$ as follows:

$$\begin{aligned} \alpha_n(V_{\mathrm{bd}}) &= \frac{0.00049(V_{\mathrm{bd}}-32)}{1-\exp(-(V_{\mathrm{bd}}-32)/25)}, \\ \beta_n(V_{\mathrm{bd}}) &= \frac{0.00008(V_{\mathrm{bd}}-42)}{\exp((V_{\mathrm{bd}}-42)/10)-1}. \end{aligned}$$

For the NMDA-mediated channel I_{NMDA}, there is a marked voltage dependency in the presence of extracellular Mg^{2+}. For physiological Mg^{2+} concentration, the voltage dependence of I_{NMDA} can be described as follows:

$$B(V_{\mathrm{bd}}) = \frac{1}{1+0.2801\exp(-0.0744V_{\mathrm{bd}})}.$$

REFERENCES

[1] K. Gadhoumi, J.-M. Lina, F. Mormann, and J. Gotman, "Seizure prediction for therapeutic devices: A review," *Journal of Neuroscience Methods*, vol. 260, pp. 270–282, 2016.

[2] F. Rosenow and H. Lüders, "Presurgical evaluation of epilepsy," *Brain*, vol. 124, no. 9, pp. 1683–1700, 2001.

[3] C. A. Schevon, S. A. Weiss, G. McKhann, R. R. Goodman, R. Yuste, R. G. Emerson, and A. J. Trevelyan, "Evidence of an inhibitory restraint of seizure activity in humans," *Nature Communications*, vol. 3, no. 1, p. 1060, 2012.

[4] M. Zhang, R. S. Shivacharan, C. C. Chiang, L. E. Gonzalez-Reyes, and D. M. Durand, "Propagating neural source revealed by doppler shift of population spiking frequency," *Journal of Neuroscience*, vol. 36, no. 12, pp. 3495–505, 2016.

[5] C. C. Chiang, X. Wei, A. K. Ananthakrishnan, R. S. Shivacharan, L. E. Gonzalez-Reyes, M. Zhang, and D. M. Durand, "Slow moving neural source in the epileptic hippocampus can mimic progression of human seizures," *Scientific Reports*, vol. 8, no. 1, p. 1564, 2018.

[6] A. N. Vattikonda, M. Hashemi, V. Sip, M. M. Woodman, F. Bartolomei, and V. K. Jirsa, "Identifying spatio-temporal seizure propagation patterns in epilepsy using bayesian inference," *Communications Biology*, vol. 4, no. 1, p. 1244, 2021.

[7] P. N. Modur, T. W. Vitaz, and S. Zhang, "Seizure localization using broadband eeg: Comparison of conventional frequency activity, high-frequency oscillations, and infraslow activity," *Journal of Clinical Neurophysiology*, vol. 29, no. 4, pp. 309–319, 2012.

[8] J. F. Téllez-Zenteno, R. Dhar, and S. Wiebe, "Long-term seizure outcomes following epilepsy surgery: a systematic review and meta-analysis," *Brain*, vol. 128, no. 5, pp. 1188–1198, 2005.

[9] R. S. Shivacharan, C. C. Chiang, M. Zhang, L. E. Gonzalez-Reyes, and D. M. Durand, "Self-propagating, non-synaptic epileptiform activity recruits neurons by endogenous electric fields," *Exp Neurol*, vol. 317, pp. 119–128, 2019.

[10] G. R. Holt and C. Koch, "Electrical interactions via the extracellular potential near cell bodies," *Journal of Computational Neuroscience*, vol. 6, no. 2, pp. 169–184, 1999.

[11] C. A. Anastassiou, R. Perin, H. Markram, and C. Koch, "Ephaptic coupling of cortical neurons," *Nature Neuroscience*, vol. 14, no. 2, pp. 217–23, 2011.

[12] M. Zhang, T. P. Ladas, C. Qiu, R. S. Shivacharan, L. E. Gonzalez-Reyes, and D. M. Durand, "Propagation of epileptiform activity can be independent of synaptic transmission, gap junctions, or diffusion and is consistent with electrical field transmission," *Journal of Neuroscience*, vol. 34, no. 4, pp. 1409–19, 2014.

[13] C. C. Chiang, R. S. Shivacharan, X. Wei, L. E. Gonzalez-Reyes, and D. M. Durand, "Slow periodic activity in the longitudinal hippocampal slice can self-propagate non-synaptically by a mechanism consistent with ephaptic coupling," *The Journal of Physiology*, vol. 597, no. 1, pp. 249–269, 2019.

[14] D. M. Durand, W. M. Grill, and R. Kirsch, *Electrical stimulation of the neuromuscular system*. Springer, 2005, pp. 157–191.

[15] C. Qiu, R. S. Shivacharan, M. Zhang, and D. M. Durand, "Can neural activity propagate by endogenous electrical field?" *Journal of Neuroscience*, vol. 35, no. 48, pp. 15 800–11, 2015.

[16] E.-H. Park, E. Barreto, B. J. Gluckman, S. J. Schiff, and P. So, "A model of the effects of applied electric fields on neuronal synchronization," *Journal of Computational Neuroscience*, vol. 19, no. 1, pp. 53–70, 2005.

[17] K. Lauderdale, T. Murphy, T. Tung, D. Davila, D. K. Binder, and T. A. Fiacco, "Osmotic edema rapidly increases neuronal excitability through activation of nmda receptor-dependent slow inward currents in juvenile and adult hippocampus," *ASN Neuro*, vol. 7, no. 5, 2015.

[18] M. Subramanian, C. C. Chiang, N. H. Couturier, and D. M. Durand, "Theta waves, neural spikes and seizures can propagate by ephaptic coupling in vivo," *Exp Neurol*, vol. 354, p. 114109, 2022.

[19] S. Coombes, "Neuronal networks with gap junctions: A study of piecewise linear planar neuron models," *SIAM Journal on Applied Dynamical Systems*, vol. 7, no. 3, pp. 1101–1129, 2008.

[20] E. H. Park and D. M. Durand, "Role of potassium lateral diffusion in non-synaptic epilepsy: a computational study," *J Theor Biol*, vol. 238, no. 3, pp. 666–82, 2006.

[21] D. Golomb, C. Yue, and Y. Yaari, "Contribution of persistent na+ current and m-type k+ current to somatic bursting in ca1 pyramidal cells: combined experimental and modeling study," *Journal of neurophysiology*, vol. 96, no. 4, pp. 1912–1926, 2006.